X-Ray Emission and Absorption Spectroscopy with Binary Amorphous Alloys from the B-Co-, B-Ni-, Co-P-, Co-Ti-, Cu-Mg-, Cu-Ti-, Mg-Zn-, Ni-P-, and Ni-Ti-Systems

S. Falch, P. Lamparter, and S. Steeb
Max-Planck-Institut für Metallforschung, Institut für Werkstoffwissenschaften, Seestraße 92, Stuttgart

Z. Naturforsch. **39a**, 1175–1183 (1984); received September 13, 1984

X-ray emission and absorption spectroscopy has been used to determine the partial density of occupied and unoccupied states in various metallic glasses. The X-ray emission spectra also indicate a possible electronic charge transfer between the alloyed atoms. The experiments were done by means of an electron microprobe. Amorphous Mg_2Cu was prepared by ionic sputtering, the glasses of the Mg-Cu-, Mg-Zn-, Cu-Ti-, Co-Ti-, Co-B-, Co-P-, Ni-Ti-, Ni-B-, and Ni-P-systems by the melt-spinning method.

From the measurements it is concluded that the amorphous phase is stabilized by compound formation. A combination with results of X-ray diffraction measurements on amorphous Mg_2Cu indicates that the glassy structures should be favoured by a correlation between the atoms of higher electronegativity. The shape of the density of unoccupied states vs. energy curve shows that the local symmetry around the Zn- and Cu-atoms in the amorphous phases differs from that in the corresponding crystalline phases. For the transition-metalloid glasses evidence for a fcc-like local short range order is found.

Introduction

In [1] we reported on the determination of the electronic structure of binary amorphous alloys by means of X-ray-emission spectroscopy within an electron microprobe. In the present paper X-ray absorption spectroscopy was also used. It was found that by means of an electron microprobe it is possible to obtain X-ray absorption spectra with sufficient resolution to detect the fine structure of the absorption edge. Thus one obtains access to the calculation methods of XANES [2] (**X**-ray-**A**bsorption-**N**ear-**E**dge-**S**tructure) and thereby information about the atomic arrangement of triplets. Together with the diffraction methods there are now two complementary methods available.

From one or more X-ray-emission spectra mainly three types of information are obtained:

i) With two emission-spectra, measured at different energies of the primary electrons, an absorption spectrum can be calculated.
ii) From emission spectra the charge transfer can be determined.
iii) From the shape and position of the emission lines follows the binding energy of the electrons.

Furthermore, it should be noted that the results obtained by X-ray emission spectroscopy are always characteristic for the special element, in contrast to electron spectroscopy, for example, where no direct evidence is available concerning the origin of the electron under observation.

Reprint requests to Prof. Dr. S. Steeb, Max-Planck-Institut für Metallforschung, Institut für Werkstoffwissenschaften, Seestraße 92, D-7000 Stuttgart 1.

Fundamentals of the Method

Quantum mechanical considerations [3] lead to following relation between the intensity $I(\nu)$ of X-ray emission and the density of states $D(E)$:

$$I(\nu) \sim \nu^3 W(E) D(E), \quad (1)$$

where ν = frequency of X-rays, E = electron energy, $W(E)$ = quantity which is proportional to the transition probability.

Thus from the shape of $I(\nu)$ one obtains a picture of the local partial density of states because generally the positions of the energy levels of the elements differ. Corresponding to the case of X-ray emission,

0340-4811 / 84 / 1200-1175 $ 01.30/0. – Please order a reprint rather than making your own copy.

the X-ray absorption coefficient is

$$\mu(E) \sim P(E)\, D(E)\,, \tag{2}$$

where $E > E_{\text{Fermi}}$ and $P(E)$ is porportional to the value of the matrix element of the transition probability.

Figure 1 shows schematically the method of self-absorption spectroscopy by means of electron microprobe. For the determination of $\mu(E)$ two emission spectra (I_1, I_2) are needed, where I_1 is produced by electrons with 3 keV electron energy just below the sample surface and I_2 by electrons with 25 keV electron energy from the depth $x \sin\alpha$. The X-rays in the latter case are absorbed partly along the path x. In the lower part of Fig. 1 one can see $I_1(E)$, $I_2(E)$, and $\mu(E)$, which results from

$$\mu(E) = \frac{1}{x} \ln \frac{I_1}{I_2}\,. \tag{3}$$

Exact measurements show that the increase of the absorption coefficient at the absorption edge is not discontinuous but features a structure (see Fig. 2) which represents mainly the local partial density of states and is known as "Kossel-Struktur" [4]. For example there appears a step as well as other structures in the absorption edge of transition metals, which are related to the unoccupied part of the 3d- and 4s-bands.

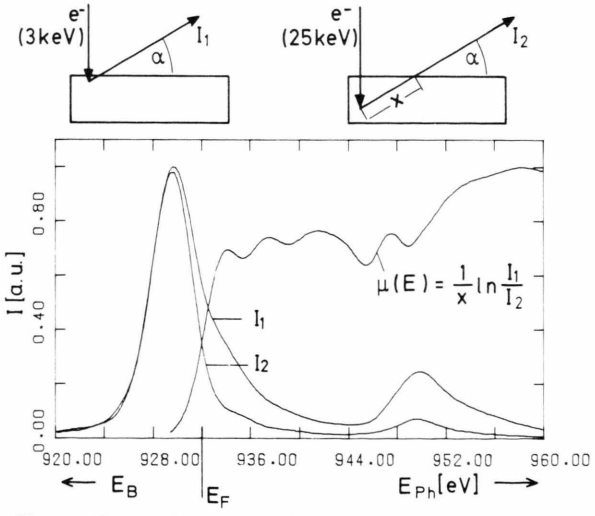

Fig. 1. Above: Geometric situation for $\mu(E)$-determination. Below: Two Cu-$L_{\gamma,\beta}$-emission spectra and resulting absorption spectrum $\mu(E)$. Emission line at 928 eV.

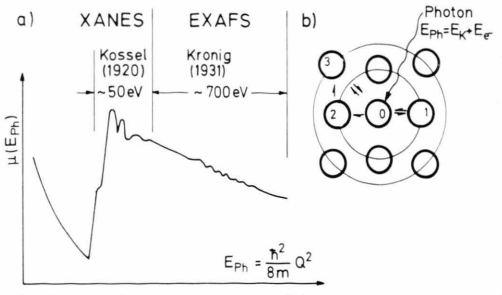

Fig. 2. a) Absorption edge with Kossel- and Kronig-fine-structure. b) Atomic arrangement (schematically): accomplishment of the EXAFS- resp. XANES-spectra by pair-(0−1) resp. triple-(0−2−3) interaction.

Within the range of a few 100 eV above the edge, an oscillating modulation of the absorption coefficient can be observed which is called "Kronig-Struktur", and which can only be observed with atoms in condensed matter [5]. In this region of the spectra (EXAFS = **E**xtended-**X**-ray-**A**bsorption-**F**ine-**S**tructure), a variation of the matrix element of the transition probability is caused by the interaction of the electron with the atoms surrounding the absorbing atom as is shown, for example, in Figure 2. An extension of this theory takes into account multiple scattering and is therefore able to give information about triple correlations (Fig. 2: atoms 0, 2, 3) [2, 6, 7]. It allows the calculation of absorption spectra in the region of 0−50 eV above the Fermi level (XANES = **X**-ray-**A**bsorption-**N**ear-**E**dge-**S**tructure). A detailed description of the determination of absorption spectra is found in [8].

A measure of the type and strength of the chemical bonding between atoms of different species is given by the so-called charge transfer. According to [9, 10] the relative variation of the number of electrons in the 3d-band of a transition metal within a sphere around the specific atom can be calculated from emission spectra:

$$\Delta n_{3d}/n_{3d} = R - 1\,. \tag{4}$$

This means that the change Δn_{3d} of the number of 3d-electrons is related to the corresponding number of 3d-electrons of a pure transition metal n_{3d}. The value R results from the equation

$$R = \left|\frac{I^{\text{int}}_{L_2}}{I^{\text{int}}_{L_1}}\right|_{\text{alloy}} : \left|\frac{I^{\text{int}}_{L_2}}{I^{\text{int}}_{L_1}}\right|_{\text{elem}} = \frac{n^i_{3d}\ \text{alloy}}{n^i_{3d}\ \text{element}} \tag{5}$$

with

$I_{L_\alpha}^{int}$ = integrated intensity of the L_α-emission line ($3d\text{-}2p^{3/2}$),

$I_{L_l}^{int}$ = integrated intensity of the L_l-emission line ($3s\text{-}2p^{3/2}$).

For the determination of R, the two integrated intensities have to be measured for the considered element in the alloyed state and the pure state. In (5) it is assumed that the 3s-level is completely filled and not influenced by the chemical surrounding. Therefore, $I_{L_l}^{int}$ can be used as reference signal to normalize the measured data. From the relative charge transfer, calculated corresponding to (4) and (5) one can obtain the change of the number of 3d-electrons in the d-band within a sphere surrounding an atom in the alloy, with respect to the number of 3d-electrons in the element.

In binary alloys containing one or two transition metal elements, the measured charge transfer has its origin in a self charge transfer or in a change of the localization of the 3d-electrons, i.e. a change of the matrix element of the transition probability after alloying.

In alloys which are composed of atoms with high electronegativity and electron density and atoms with lower electronegativity and electron density, the screening charges are redistributed [11, 12]. The screening charge is concentrated at the core of the electropositive ion to compensate for the electron transfer resulting from the difference of the electronegativities and to maintain charge neutrality of the pseudoatoms. Around the electronegative atom the opposite effect shows up. The redistribution of the screening charges acts upon the interatomic potentials in such a way that the electropositive atoms are compressed while electronegative atoms are slightly expanded. The effect is well-known as "chemical compression" [13].

Experiments

The basic alloys for the metallic glasses, for the crystalline compounds used for comparative measurements and for the sputter-target were melted with an induction furnace in an argon atmosphere (200 – 400 Torr). A graphite mould gave a good result for the Mg_2Cu target. To get maximum homogeneity, the crystalline samples were annealed in a glow furnace. The metallic glasses were prepared as ribbons with a selfmade melt-spin apparatus [14].

By means of RF-sputtering, Mg_2Cu was produced as an amorphous foil with a thickness of about 10 μm. The measurements were done with an electron microprobe (Jeol JXA-733) with two focusing linear spectrometers. The whole counting- and controlling-electronics as well as the data processing were supervised by a computer. Thus it was possible to process the measured values and to save them on disk while on the other hand the computer controlled the measuring process.

The X-ray emission spectra were recorded from both components in the metallic glasses, in the crystalline phases and in the pure elements, if possible.

For transitions out of the valence levels the L_α- and L_β-spectra were measured, while the K_β-spectra were measured in the case of magnesium and phosphorus. For the normalization in the calculation procedure of the charge transfer the L_l-spectrum was also recorded. The spectrometer stepwidth normally was 0.04 mm, in the case of sufficient intensity it was 0.02 mm. Using a TAP-crystal in the range of $\lambda = 13$ Å this is equivalent to about $3.7 \cdot 10^{-3}$ Å and $1.85 \cdot 10^{-3}$ Å, respectively. The counting time for each spectrometer step was selected in such a way as to minimize the resulting error caused by the drift of the apparatus and the surface contamination, and to get a sufficient count rate. The spectrometer resolution $\frac{\Delta\lambda}{\lambda}$ is about 10^{-3}.

The spectra were smoothed according to the method of cubic spline fit and deconvoluted with an experimentally determined instrumental resolution function. The position of the Fermi level, which is the zero of the energy scale, was taken as the position of the inflection point of the absorption edge.

Results and Discussion

In order to compare the results obtained with amorphous alloys, measurements with pure elements were also done. They also could be compared with results obtained with other spectroscopic methods. The spectra obtained with pure copper were shown already in Figure 1. The emission spectrum is designated as I_1 and is plotted versus the energy. On the abscissa the position of the Fermi level is marked, and also the direction of increasing electron

binding energy. The curve corresponds to the density of states in the occupied part of the d-band (I_1) below E_F, as well as to the unoccupied states ($\mu(E)$) above E_F. The maxima in the density of unoccupied states result from flat bands at high symmetry points of the Brillouin zone [12]. The critical point energies of copper are in good agreement with those from theoretical bandstructure calculations [15].

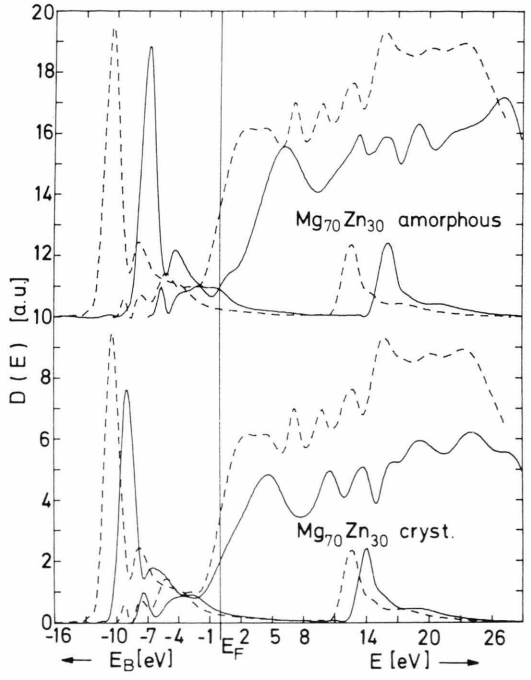

Fig. 3. Mg-Zn system: partial density of Zn-states from Zn L-spectra, ——— alloy, – – – – pure zinc (hcp).

Mg-Zn-system

With Mg-Zn as a system of simple metals one has the possibility to compare a crystalline phase with an amorphous phase, both with the same composition. Figure 3 shows the results from measurements of the crystalline phase $Mg_{70}Zn_{30}$ and of the amorphous phase $Mg_{70}Zn_{30}$, in each case compared to pure zinc. The density of occupied states vs. energy curve shows in the case of the crystalline and amorphous phase the same shape but not the same position of the peak as was obtained with pure zinc. The distance of the 3d-peak to the Fermi level decreases from pure zinc to the crystalline phase, and further to the amorphous phase. The measured spectra are in accordance to those from [16]. The density of unoccupied states is different in the crystalline phase compared to the amorphous phase and to pure zinc.

Figure 4 shows the Mg K_β-emission spectra for crystalline and amorphous $Mg_{70}Zn_{30}$, in each case compared to crystalline Mg. The spectra of the alloys, measured with 25 kV (Fig. 4b) show in contrast to the spectra measured with 5 kV (Fig. 4a) a pronounced intensification of the high energy peak, which is shifted by about 1 eV to higher binding energies with the alloys in Fig. 4a. The experimental fact that the solid lines in Fig. 4 show

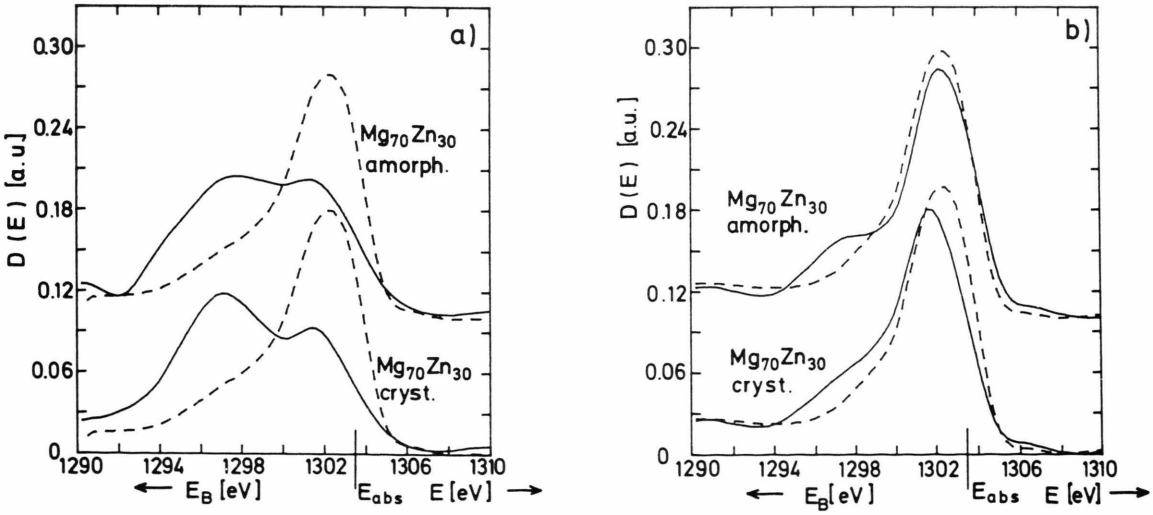

Fig. 4. Mg-Zn system: partial density of Mg-states from Mg-K_β-spectra, ——— alloy, – – – – pure magnesium. a) Accelerating voltage 5 kV, b) accelerating voltage 25 kV.

Table 1. Mg-Zn system. Values of binding energy $E_B(L_{III})$ and $E_B(3d)$ as well as of charge transfer Δn.

Alloy	$E_B(L_{III})$ [eV]	$E_B(3d)$ [eV]	$\Delta n/n$	Δn
$Mg_{70}Zn_{30}$ (cryst.)	−1023.4	− 9.0	0.05	0.5
$Mg_{70}Zn_{30}$ (amorph.)	−1018.6	− 6.6	0.01	0.1
Zn (cryst.)	−1022.0	−10.3	–	–

drastical changes in dependence on the accelerating voltage whereas the dashed lines corresponding to elementary Mg remain nearly unchanged is not to be explained by absorption effects. In a distance of about 4.5 eV to the high energy peak, an additional peak at higher binding energies appears. This can be understood as an hybridization of Mg 3p-states with Zn-states just below the Fermi-boundary. Let us remark that the free Mg-atom has two 3s-valence electrons, which in the solid state can occupy 3s- as well as 3p-states.

To interprete the Mg-peak at lower energies as a transition from the Zn 3d-band analogous to transition-metal-magnesium-alloys [17] would not be in accordance with the distance of the zinc 3d-band to the Fermi level.

Table 1 contains the binding energies for the L_{III} ($2p^{3/2}$)-level, for the maximum of the 3d-band as well as the values for the relative and the absolute charge transfer under the assumption of 10 d-electrons in crystalline zinc. A small positive amount of charge transfer to the zinc atom is in accordance with the electronegativity difference of 0.4. The difference in the values of the charge transfer for amorphous $Mg_{70}Zn_{30}$ and crystalline $Mg_{70}Zn_{30}$ is consistent with the corresponding distance of the 3d-band to the Fermi-energy. The reason for the change of the spectra when increasing the accelerating voltage from 5 kV to 25 kV has yet to be clarified. Because of the relative decrease of the peak at lower energies in the Mg-K_β-spectra, it is not possible to determine from these spectra the shape of the absorption coefficient.

The present measurement indicate a stabilization of the amorphous system by compound formation between magnesium and zinc atoms similar to the crystalline phase. Because in the two alloys the density of unoccupied states shows only a small difference in the form of the second maximum (apart from the position of the Fermi-level), one can conclude that the surrounding of a zinc atom in amorphous $Mg_{70}Zn_{30}$ is similar to that in crystalline $Mg_{70}Zn_{30}$. This indicates that there is compound formation in the amorphous phase like in the crystalline phase as a stabilizing moment. In [11] it is shown that a variation of the screening charges causes a change of the interatomic potentials in such a way that there is a stabilizing interaction between the atoms of the electronegative alloy component. Accordingly the screening charge density at the zinc atom in the amorphous alloy should be smaller than in the crystal. An indication for this is the smaller amount of charge transfer in amorphous $Mg_{70}Zn_{30}$ compared to crystalline $Mg_{70}Zn_{30}$. An accompanying "compression" of the Mg atoms and correspondingly an extension of the Zn atoms causing a small change of the local atomic structure could be the reason for the slight difference in the shape of the density of unoccupied states.

Mg-Cu-system

Figure 5 shows the curves of the local partial copper density of states from the alloys $MgCu_2$, Mg_2Cu, Mg_2Cu (amorphous) and $Mg_{86}Cu_{14}$ (amorphous), each compared to the one from crystalline copper, resulting from measurements of the L_{III}-emission and -absorption spectra. The critical point energies for copper, taken from ref. [15], are also

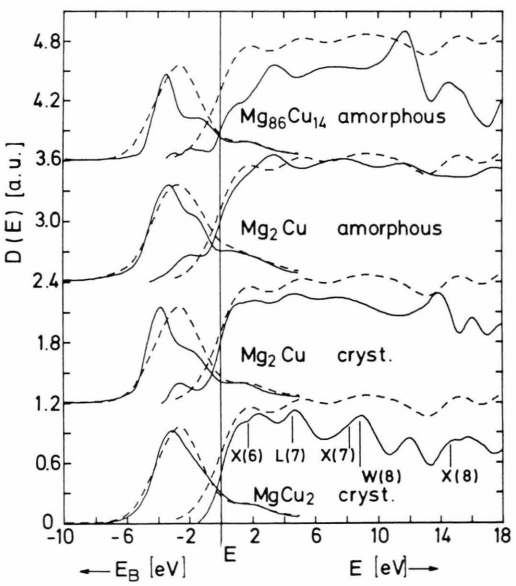

Fig. 5. Mg-Cu system: partial density of Cu-states from Cu L-spectra, ——— alloy, – – – – pure copper (fcc).

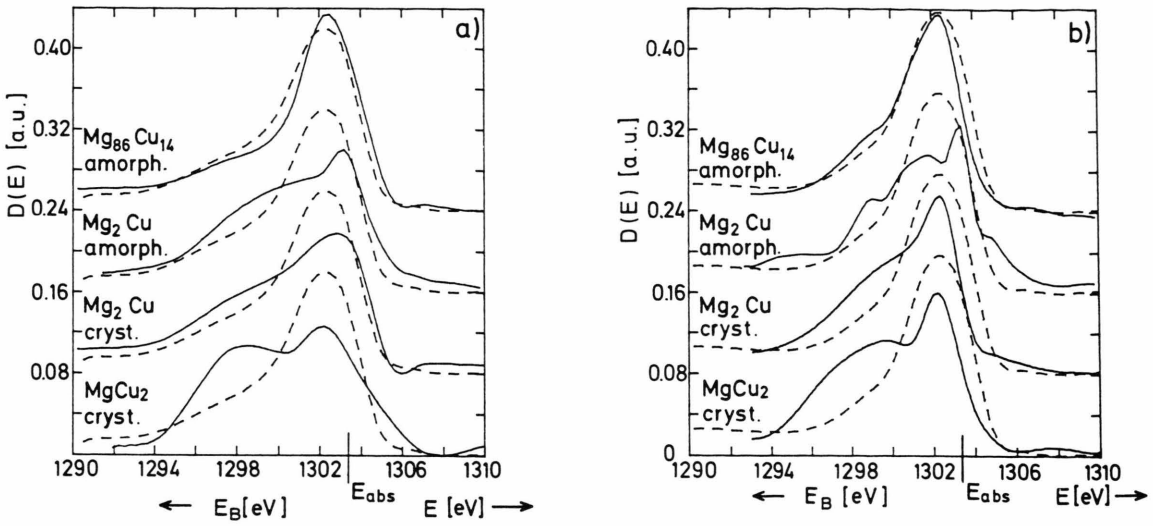

Fig. 6. Mg-Cu system: partial density of Mg-states from Mg-K$_\beta$-spectra, ——— alloy, - - - - pure magnesium. a) Accelerating voltage 5 kV, b) accelerating voltage 25 kV.

Table 2. Mg-Cu system. Values of binding energy $E_B(L_{III})$ and $E_B(3d)$ as well as of the charge transfer Δn.

Alloy	$E_B(L_{III})$ [eV]	$E_B(3d)$ [eV]	$\Delta n/n$	Δn
$MgCu_2$ (cryst.)	−932.5	−3.07	−0.09	−0.85
Mg_2Cu (cryst.)	−932.8	−3.76	−0.15	−1.4
Mg_2Cu (amorph.)	−932.6	−3.25	−0.05	−0.5
$Mg_{86}Cu_{14}$ (amorph.)	−932.55	−3.46	−0.07	−0.65
Cu (cryst.)	−932.3	−2.6	–	–

shown. In the alloys the copper 3d-peak is shifted to higher binding energies, where the d-band maximum of crystalline Mg_2Cu shows the largest distance to the Fermi-level. The values for pure copper (2,6 eV) is in exact accordance with ref. [18]. At the binding energy of about 1.65 eV one can recognize a shoulder which grows with increasing magnesium content. The shape of the density of unoccupied states is clearly different for the amorphous and the crystalline alloys. It is remarkable that in the case of the amorphous alloys up to 8 eV the curves are rather similar to each other. From this one can conclude that the symmetry in the surrounding of the corresponding copper atoms is also rather similar.

The positions of the critical point energies in the density of unoccupied states in $MgCu_2$ are in sufficient accordance with those in pure copper. Both substances have a fcc lattice structure with a small difference in the lattice constant (a(Cu) = 6.76 Å [19], $a(MgCu_2)$ = 7.047 Å [20]). The orthorhombic Mg_2C, however, diverges clearly.

Figure 6 shows the partial magnesium density of states in these alloys compared with the density of states in pure magnesium, measured at an electron accelerating voltage of 5 kV (Fig. 6a) and 25 kV (Figure 6b). The partial density of states shows in each case in the region around 1298 eV a shoulder which grows with increasing copper content. In addition there is a small shift to lower binding energies for crystalline Mg_2Cu as well as for amorphous Mg_2Cu. The influence of a higher accelerating voltage on the measured magnesium density of states (compare Fig. 6b) is much lower than in the Mg-Zn system treated before.

The magnesium valence band consists of overlapping 3s- and 3p-states. Because of the transition probability the magnesium K$_\beta$-spectrum results from transitions of electrons out of p-states. The 3s part of the spectra increases with higher copper concentration. Combined with the variation of the copper 3d-band, this is an indication of a hybridization between magnesium 3p- and copper 3d-orbitals in the upper part of the d-band, i.e. compared with the Mg-Zn system at higher binding energies.

The values of the binding energies and of the charge transfer, which result from the partial copper density of states are shown in Table 2. In sputtered amorphous Mg_2Cu the copper 3d-peak as

well as the magnesium 3p-peak are positioned at lower binding energies than in crystalline Mg_2Cu. With regard to the Mg-Cu interaction this means a weaker electronic stabilization of the sputtered alloy compared to crystalline Mg_2Cu but also compared to melt-spun amorphous $Mg_{86}Cu_{14}$. The negative values for the charge transfer could mean that the copper atoms contribute electrons to the binding. This negative charge transfer being smaller in amorphous alloys with comparable concentration ratios cannot be explained by the electronegativity difference between magnesium and copper.

It could be possible that because of a change in the symmetry of the d-electrons, caused by hybridization, the transition probability ($3d-2p^{3/2}$) has decreased. In [1] a splitting of the density of states of the copper 3d-band in the Zr-Cu system was reported as well and has been explained by an overlapping of copper and zirconium d-states. The shift of the d-band towards higher binding energies was found to be in accordance with the difference of the electronegativity between the two alloy constituents.

However, in the Mg-Cu system the shift of the 3d-band towards higher binding energies is much smaller than in the Zr-Cu system, although the difference of the electronegativities is larger by 0.2.

Combined with the data from Table 2 and the results from diffraction experiments [8] this indicates that in the case of Mg-Cu alloys there is not simply a charge transfer present but rather a screening effect, i.e. the electronic charge of the electronegative copper atom screens the electropositive magnesium atom where the latter is correspondingly compressed. The similar shape of the density of unoccupied states of copper in amorphous Mg_2Cu and $Mg_{86}Cu_{14}$ indicates that the symmetry around the copper atoms in both alloys is similar. The statement in [21] that the local structure around the Cu atoms in amorphous $Mg_{86}Cu_{14}$ is similar to the one in crystalline Mg_2Cu, might not hold for the case of amorphous Mg_2Cu because of the difference of the copper density of states in the range $E > E_F$ in amorphous and crystalline Mg_2Cu.

In many metallic glasses the interatomic distances are dependent on the concentration ratio. With increasing concentration of the more electronegative atomic species the distance between atoms with lower electronegativity decreases as well as the distance between more and lower electronegative atoms [11]. This "compression" of electropositive atoms results from the charge transfer which is caused by orthogonalization- and screening-effects as mentioned above.

In the considered Mg-Cu system this would mean that in the amorphous alloys the Mg-Mg distances and the Mg-Cu distances should decrease slightly with increasing copper content. This is confirmed by results from diffraction experiments [8]. In this case the experimental results indicate as well that the metallic glasses of the Mg-Cu system are stabilized by compound formation between the Mg- and the Cu-atoms and by interaction between copper atoms. This means the Cu atoms are located at the minima of their pair potentials which stabilizes the amorphous state.

Ni-B, Ni-P, Ni-Ti, as well as Co-B, Co-P, Co-Ti, and Cu-Ti systems

Table 3 shows the characteristic energy values and the charge transfer for the Ni-, Cu-, and Co-d-band. In the Cu-Ti alloys the negative charge transfer disappears with increasing Ti-content, which can be attributed to screening effects. Combined with the measured density of unoccupied states (compare Fig. 34 in [8]) one can conclude that an increasing tendency to isotropical arrangement of the atoms is connected with a decreasing tendency in transferring binding electrons.

It is remarkable that in the case of similar alloys the charge transfer to the Ni-d-band is smaller than to the Co-d-band. This means that the Ni atoms accept fewer electrons than the Co atoms. This

Table 3. Co-B, Co-P, Co-Ti as well as Ni-B, Ni-P, Ni-Ti, and Cu-Ti systems. Values of binding energies $E_B(L_{III})$ and $E_B(3d)$ as well as of the charge transfer Δn.

Alloy	$E_B(L_{III})$ [eV]	$E_B(3d)$ [eV]	$\Delta n/n$	Δn
$Co_{80}B_{20}$ (amorph.)	−777.5	−1.15	0.25	1.83
$Co_{80}P_{20}$ (amorph.)	−777.7	−1.53	0.24	1.75
$Co_{74}Ti_{20}B_6$ (amorph.)	−777.6	−1.3	0.23	1.68
$Co_{25}Ti_{75}$ (amorph.)	−777.7	−1.53	0.4	2.9
Co (cryst.)	−777.0	−0.85	–	–
$Cu_{73}Ti_{27}$ (amorph.)	−932.0	−3.0	−0.09	−0.9
$Cu_{67}Ti_{33}$ (amorph.)	−932.7	−3.53	−0.02	−0.2
$Cu_{50}Ti_{50}$ (amorph.)	−932.7	−3.6	0.0	0.0
Cu (cryst.)	−932.3	−2.6	–	–
$Ni_{80}P_{20}$ (amorph.)	−853.2	−1.3	0.08	0.67
$Ni_{80}B_{20}$ (amorph.)	−852.0	−0.9	0.06	0.5
Ni_2P (cryst.)	−853.0	−1.4	0.24	2.0
$Ni_{40}Ti_{60}$ (amorph.)	−853.8	−2.0	0.24	2.0
Ni (cryst.)	−853.0	−1.45	–	–

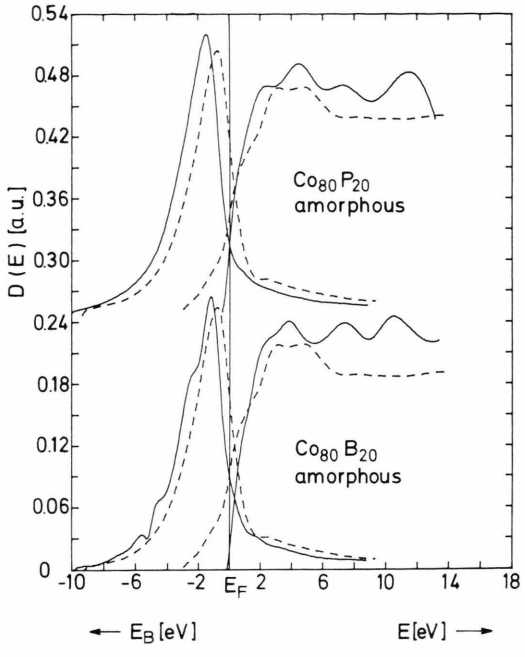

Fig. 7. $Co_{80}P_{20}$ amorphous resp. $Co_{80}B_{20}$ amorphous: partial density of Co-states from Co L-spectra, ——— alloy, - - - - pure cobalt (hcp).

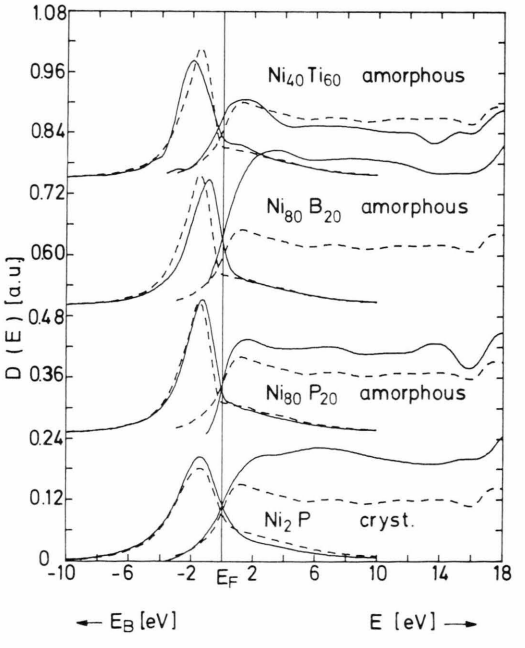

Fig. 8. Various Ni-alloys: partial density of Ni-states from Ni L-spectra, ——— alloy, - - - - pure nickel.

tendency can be explained by the smaller amount of free states in the Ni-d-band in contrast to the Co-d-band. From results of magnetic measurements it can also be concluded that d-states of transition metals can be occupied by electrons of the metalloid atoms [22, 23]. Compton spectra from Co-P and Ni-P show the same results [24], but the absolute values are smaller compared to those from the present measurements.

Figure 7 shows the shape of the partial density curve of Co-states in amorphous $Co_{80}B_{20}$ and amorphous $Co_{80}P_{20}$, in each case compared to crystalline Co. Compared to pure Co, all amorphous Co-alloys show a slight increase in the binding energy of the 3d-band. Additionally with the disappearance of the shoulder in the absorption spectrum at the Fermi edge, this corresponds to a charge transfer to the Co 3d-band which means that the band is filled up. It should be noted that the alloys containing Ti show a smaller structure in the partial Co density of unoccupied states compared, for example, to the shapes in Figure 7. A similar effect has already been discussed in the case of the Cu-Ti alloys and was interpreted as a tendency to a more isotropical atomic arrangement. The structure in the absorption spectra of amorphous $Co_{80}B_{20}$ and $Co_{80}P_{20}$ is nearly the same, but compared to that of pure Co it is completely different. The position of the maxima in the absorption spectra of the $Co_{80}B_{20}$ and $Co_{80}P_{20}$ alloys are in good accordance with those of crystalline Ni (Fig. 8) and crystalline Cu (Figure 5). This may be an indication for a fcc-symmetry in the surrounding of the Co-atoms (compare [25]).

Figure 8 shows the partial Ni density of states in crystalline Ni_2P(hcp), amorphous $Ni_{80}P_{20}$, amorphous $Ni_{80}B_{20}$, and amorphous $Ni_{40}Ti_{60}$, where the density of states in crystalline Ni is drawn as dashed curve. The Ni d-bands of the alloys are mostly shifted and slightly broadened compared to those of pure crystalline Ni. this is mainly caused by the charge transfer, but it should be noticed that a change in the exchange splitting could counteract the broadening. Additionally it should be mentioned that Ni 3d-bands with small positive charge transfer are shifted towards lower binding energies. In the case of amorphous $Ni_{60}Ti_{40}$, from the broadening and simultaneous shift of the 3d-band towards lower binding energies combined with the charge transfer a hybridization between Ni- and Ti-d-states can be concluded.

Above E_F, the shape of the density of states in $Ni_{80}P_{20}$ is very similar to that of crystalline Ni. Crystalline Ni shows a structure which is characteristic for fcc-symmetry [26] and corresponds to the results from SXAPS measurements [27].

The P-K_β-spectra are shown in [7], where the partial density of P-states in crystalline Ni_2P, amorphous $Ni_{80}P_{20}$, and amorphous $Co_{80}P_{20}$ are compared to the shape of the density of states in pure phosphorus. In the amorphous alloys the P-peak is shifted towards higher binding energies. The measured charge transfer is in sufficient accordance with magnetic measurements [23]. But it can not be distinguished whether the most important part is played by screening effects, hybridization (i.e. strong compound formation) or a real charge transfer to the d-band of an alloy constituent.

[1] S. Falch, G. Rainer-Harbach, F. Schmückle, and S. Steeb, Z. Naturforsch. **36a,** 937 (1981).
[2] P. J. Durham, J. B. Pendry, and C. H. Hodge, Solid-state Com. **38,** 159 (1981).
[3] L. V. Azároff, X-Ray-Spectroscopy, McGraw-Hill, New York 1974, Chapt. 4.
[4] W. Kossel, Z. Phys. **1,** 119 (1920).
[5] R. de L. Kronig, Z. Phys. **70,** 317 (1931); ibid. **75,** 191 (1932); ibid. **75,** 468 (1932).
[6] P. H. Gaskell, D. M. Glover, A. K. Livesey, P. J. Durham, and G. N. Greaves, J. Phys. C **15,** 597 (1982).
[7] P. J. Durham and J. B. Pendry, Computer Physics Communications **25,** 193 (1982).
[8] S. Falch, Doctor-Thesis, University of Stuttgart 1983.
[9] A. Wenger, Doctor-Thesis, Lausanne 1971.
[10] A. Wenger and S. Steinemann, Helvetica Physica Acta **47,** 321 (1974).
[11] J. Hafner, Phys. Rev. B **21,** 406 (1980).
[12] W. A. Harrison, Electronic Structure and the Properties of Solids, W. H. Freeman, San Francisco 1980.
[13] H. Ruppersberg and W. Speicher, Z. Naturfosch. **31a,** 47 (1976).
[14] W. Sperl, Diplom-Thesis, University of Stuttgart 1980.
[15] R. Lässer and N. V. Smith, Phys. Rev. B **24,** 1895 (1981).
[16] H. Neddermayer, in: Proceedings of the International Symposium X-Ray Spectra and Electronic Structure of Matter, A. Faessler and G. Wiech, München 1973.
[17] C. Curry and R. Harrison, Phil. Mag. **21,** 659 (1970).
[18] C. Bonnelle, in: Soft X-Ray Band Spectra and the Electronic Structure of Metals and Materials, D. J. Fabian, Academic Press, London, New York 1968.
[19] V. L. Moruzzi, J. F. Janak, and A. R. Williams, Calculated electronic Properties of Metals, Pergamon Press Inc., London 1978.
[20] E. Grime and K. Morris-Jones, Phil. Mag. **7,** 1113 (1929).
[21] E. Nassif, P. Lamparter, W. Sperl, and S. Steeb, Z. Naturforsch. **38a,** 142 (1983).
[22] R. C. O'Handley, in: Amorphous Metallic Alloys, F. E. Luborsky, Butterworth Co., London 1983.
[23] C. D. Graham and T. Egami, Ann. Rev. Mater. Sci. **8,** 423 (1978).
[24] K. Suzuki, F. Itoh, T. Honda, T. Fukunaga, and K. Ikeno, Proc. Conf. on Metallic Glasses, Science and Technology, Vol. 1, 475, Budapest 1980.
[25] V. Dose, A. Härtl, and J. Rogozik, to be published in Solid State Com.
[26] F. Szmulowicz and D. M. Pease, Phys. Rev. B **17,** 3341 (1978).
[27] V. Dose and G. Reusing, to be published in Solid State Com.